

Helicity, anisotropies and their competition in a multiferroic magnet: insight from the phase diagram

M. V. Gvozdikova,¹ T. Ziman,^{1,2} and M. E. Zhitomirsky³

¹*Institut Laue Langevin, Boîte Postale 156, F-38042 Grenoble Cedex 9, France*

²*LPMMC, UMR-5493, Université Grenoble Alpes and CNRS, 38042 Grenoble, France*

³*CEA, INAC-PHELIQS, F-38000, Grenoble, France*

(Dated: June 8, 2016)

Motivated by the complex phase diagram of MnWO_4 , we investigate the competition between anisotropy, magnetic field, and helicity for the anisotropic next-nearest-neighbor Heisenberg model. Apart from two competing exchanges, which favor a spiral magnetic structure, the model features the bi-axial single-ion anisotropy. The model is treated in the real-space mean-field approximation and the phase diagram containing various incommensurate and commensurate states is obtained for different field orientations. We discuss the similarities and differences of the theoretical phase diagram and the experimental diagram of MnWO_4 .

PACS numbers: 75.30.Kz, 75.40.Mg, 75.85.+t, 75.10.Jm

Introduction.—Phase diagrams of magnetic materials contain important information about their atomic-scale interactions. Competition between exchange interactions and anisotropy may produce nearly degenerate states that exhibit remarkable sensitivity to an applied magnetic field leading to rich and complex phase diagrams. Such a situation is often realized in spiral multiferroics, where helicity results from frustrated exchanges and a sizable spin-orbit interaction is a source of coupling between local magnetization and electric polarization [1, 2]. An incomplete list of multiferroic materials with numerous incommensurate and commensurate magnetic states includes TbMnO_3 [3, 4], $\text{Ni}_3\text{V}_2\text{O}_8$ [5–7], CeFeO_2 [8], CuO [9, 10], $\text{RbFe}(\text{MoO}_4)_2$ [11], and MnWO_4 [12–14].

Recently, significant progress was made in the reconstruction of the full phase diagram of MnWO_4 with the help of neutron diffraction [15] and electric polarization [16] measurements in pulsed magnetic fields. Despite substantial experimental [17–19] and theoretical [20–25] efforts a full explanation of the complex phase diagram of MnWO_4 is still lacking. Here we adopt a strategy different from the phenomenological theories of MnWO_4 [22–25] by formulating and studying a minimal spin model relevant to this magnetic material. The Landau energy functional for competing multi-component order parameters typically has a large number of unknown phenomenological parameters producing a significant degree of arbitrariness. Besides, the Landau theory is not applicable at low temperatures and strong magnetic fields, where interesting phase transformations take place. In contrast, the minimal spin model contains the least possible number of coupling constants and can be simulated without any *ad-hoc* assumption on equilibrium magnetic states.

In this work we investigate the anisotropic next-nearest-neighbor Heisenberg (ANNNH) spin model. In addition to competing exchange interactions the model features a *bi-axial* single-ion anisotropy, which is consistent with the monoclinic symmetry of MnWO_4 . Ba-

sically, this model is a generalization of the celebrated ANNNI model [26, 27] to three-component quantum spins. We obtain the H – T phase diagram of the ANNNH model using unrestricted real-space mean-field simulations. This approach has certain advantages in comparison to the classical Monte Carlo simulations used before for spiral multiferroics [28, 29] as it includes local quantum fluctuations and allows us to predict field and temperature variations of the ordering wave vectors (see details below). Our study suggests that the field-induced transition into the commensurate state in MnWO_4 can be produced by the bi-axial anisotropy, whose role in this was so far overlooked in the literature. The topology of the phase diagram of MnWO_4 for magnetic fields along the easy axis is perfectly reproduced within the ANNNH model.

The spin Hamiltonian of the model

$$\hat{\mathcal{H}} = \hat{\mathcal{H}}_{ex} + \hat{\mathcal{H}}_{SI}, \quad \hat{\mathcal{H}}_{ex} = \sum_{\langle ij \rangle} J_{ij} \mathbf{S}_i \cdot \mathbf{S}_j, \\ \hat{\mathcal{H}}_{SI} = \sum_i \left\{ E[(S_i^x)^2 - (S_i^y)^2] - D(S_i^z)^2 \right\} \quad (1)$$

describes an array of antiferromagnetic spin chains along the c -axis with competing first J_1 and second J_2 neighbor exchange interactions. Coupling between chains in the ab plane is assumed to be ferromagnetic $J_0 < 0$. The bi-axial single-ion anisotropy has the easy axis along z and the hard axis along x : $D > E > 0$. Note, that in low-symmetry crystals, orientation of the principal spin axes may differ from the crystallographic directions. For $J_2 > J_1/4$ and weak anisotropy, the model has a spiral magnetic ground state with the wave vector $\cos Q = -J_1/(4J_2)$ along the chain direction. This toy model is often invoked for a description of real spiral antiferromagnets [5, 30–34].

Generally, a weak easy-axis anisotropy splits a single transition temperature of an exchange spiral anti-

ferromagnet into two separate transitions for longitudinal (higher T_c) and transverse (lower T_c) spin components [31]. In addition, MnWO_4 features the third low-temperature transition into a commensurate collinear state with moments parallel to the easy axis. The extra transition appears because an exchange energy loss in the commensurate state is surpassed by a gain in the anisotropy term. In particular, this requires close values for the wave vectors in the two magnetic structures. To model such a situation in the framework of the ANNNH model, we fix $J_2/J_1 = 2$, which yields the spiral wave vector $Q_{IC}/(2\pi) = 0.27$ close to the commensurate value $Q_C/(2\pi) = 0.25$.

Theory.—To find possible ordered states of the ANNNH model in an external magnetic field \mathbf{H} we use the real-space mean-field approach; see, for example, [35, 36]. The mean-field theory begins with defining local averages $\mathbf{m}_i = \langle \mathbf{S}_i \rangle$ and neglecting intersite correlations $\langle (\mathbf{S}_i - \mathbf{m}_i)(\mathbf{S}_j - \mathbf{m}_j) \rangle = 0$ in the exchange term. In the mean-field approximation, the spin Hamiltonian transforms into

$$\hat{\mathcal{H}}_{MF} = \hat{\mathcal{H}}_{SI} - \sum_i \mathbf{h}_i \cdot \mathbf{S}_i - \sum_{\langle ij \rangle} J_{ij} \mathbf{m}_i \cdot \mathbf{m}_j, \quad (2)$$

where the local fields are $\mathbf{h}_i = \mathbf{H} - \sum_j J_{ij} \mathbf{m}_j$. Because of the single-ion anisotropy, the dependence of \mathbf{m}_i on \mathbf{h}_i is not described by the Brillouin function. Instead, we have diagonalized the local Hamiltonian matrix for a given \mathbf{h}_i and $S = 5/2$ (assuming Mn^{2+} ions) and computed \mathbf{m}_i numerically. The mean-field Hamiltonian (2) has been simulated on finite clusters with periodic boundary conditions. To match the incommensurate wave vector Q_{IC} the linear dimension along chains has to be chosen at least $L = 100$ sites. On the other hand, the commensurate $Q_{\perp} = 0$ ($J_0 < 0$) allows us to consider in the mean-field approximation only a single chain, replacing the effect of neighboring chains by an effective field.

For fixed H and T , we start with a random set of $\{\mathbf{m}_i\}$ and iterate repeatedly the self-consistency condition for all sites until convergence. The procedure is performed for up to 10^3 initial random configurations and a solution with the lowest free-energy is selected. For the obtained spin structure we calculate the Fourier harmonics m_q^α for all possible wave vectors $q = 2\pi n/L$ with integer n and pick up the maximum amplitude for each α .

Results.—Let us begin with the behavior in zero magnetic field. We have performed the real-space mean-field simulations of the model (1) with $J_1 = 1$, $J_2 = 2$ and various values for D , E , and J_0 . The role of inter-chain coupling $|J_0| \leq J_1$ consists, for the most part, of a trivial shift in all characteristic temperatures by $\Delta T = zS(S+1)|J_0|/3$, where z is the number of nearest-neighbor chains. For brevity we show only the results obtained with $J_0 = 0$. The typical behavior for a moderate anisotropy $D = 0.2$ is shown in the top panel of Fig. 1. We use the standard convention adopted for MnWO_4 and

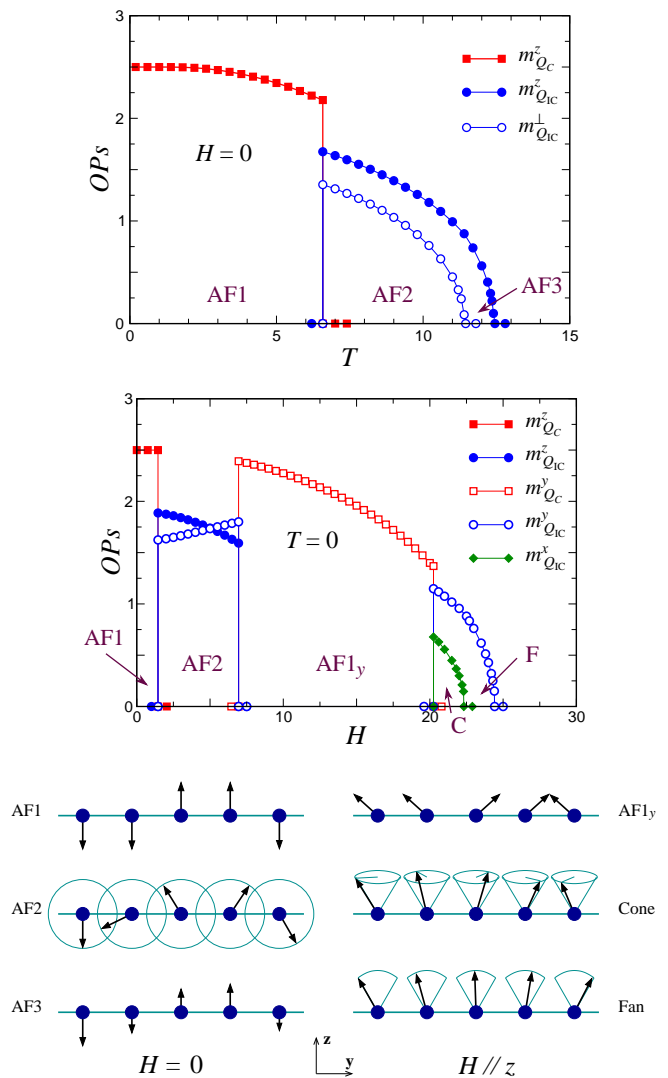


FIG. 1: Upper panel: temperature dependence of the order parameters in zero field for the uniaxial anisotropy: $D = 0.2$ and $E = 0$. Middle panel: field dependence of the order parameters at $T = 0$ in the bi-axial case: $D = 0.3$ and $E = 0.1$. Lower panel: sketch of the six states of the ANNNH model in magnetic field $\mathbf{H} \parallel z$ with corresponding labels. For illustration purpose, the easy z axis is chosen to be orthogonal to the chain c direction.

label the ordered antiferromagnetic phases from low to high temperatures as AF1, AF2, and AF3. The corresponding spin structures are sketched in the bottom panel of Fig. 1. The collinear AF1 state described by the commensurate wave vector $Q_C/2\pi = 0.25$ is stable below $T_{c1} \approx 6.6$. The elliptical spiral AF2 state exists at $T_{c1} < T < T_{c2} \approx 11.4$ and the collinear sinusoidal AF3 state appears at $T_{c2} < T < T_{c3} \approx 12.4$ with the incommensurate propagation vector $Q_{IC}/2\pi \approx 0.27$ in both cases.

Three successive transitions are present for $0.17 \lesssim D \lesssim 0.35$. For smaller anisotropy, $D \leq 0.15$, the model ex-

hibits only two transitions with the elliptical spiral state stable for all $T < T_{c2}$. For larger anisotropy, $D \geq 0.4$, the spiral phase disappears, opening up a direct transition between collinear commensurate and incommensurate states. Such a behavior is observed in iron-doped $\text{Mn}_{1-x}\text{Fe}_x\text{WO}_4$ for $x \geq 5\%$, where Fe^{2+} ions are believed to enhance the local anisotropy [36, 37].

Even though the zero-field behavior of MnWO_4 can be satisfactorily accounted for by a uniaxial anisotropy, theoretical description of field-induced states requires us to include an in-plane term E . The middle panel of Fig. 1 shows the field evolution of order parameters at $T = 0$ for $D = 0.3$ and $E = 0.1$ with the field applied along the easy axis. The magnetization process features five distinct antiferromagnetic phases before transition into the saturated state at $H_s \approx 24$. Apart from the common conical (C) and fan (F) magnetic structures [31], there is a wide region of the commensurate antiferromagnetic state with a nonzero $m_{Q_C}^y$, which we accordingly denote as the AF1_y state.

Essentially the sequence of ordered states, $\text{F} \rightarrow \text{C} \rightarrow \text{AF1}_y$, upon decreasing magnetic field at $T = 0$ repeats the sequence $\text{AF3} \rightarrow \text{AF2} \rightarrow \text{AF1}$ upon cooling in zero field with active spin components rotating in the xy and the yz planes, respectively. In particular, presence of the commensurate AF1_y state requires a substantial difference between the intermediate y axis and the hard x axis to compensate the exchange energy loss with respect to the incommensurate conical structure. The field region occupied by the AF1_y state shrinks for decreasing E and completely goes away for $E \lesssim 0.08$. In turn, the conical state disappears for $E \gtrsim 0.13$ opening a direct $\text{F} \rightarrow \text{AF1}_y$ transition. Note, that the distorted conical and the fan states both have a small longitudinal harmonic $m_{2Q_{1C}}^z$, which is a subdominant order parameter and, therefore, not included in Fig. 1.

The H - T phase diagram of the ANNNH model for the field parallel to the z axis is shown in the upper panel of Fig. 2. The obtained diagram is strikingly similar to the experimental phase diagram of MnWO_4 for fields along the easy direction [15, 16]. Since the experiments were performed in pulsed magnetic fields $H \simeq 30$ – 50 T, only the low-field states of MnWO_4 were fully characterized so far. Our theory strongly suggests that the experimental states IV and V have the conical and the fan structure, respectively. Accordingly, the magnetoelectric effect was found only in the IV (C) state [16]. The field-induced commensurate state HF [15] is identified with the AF1_y phase with moments alternating along the intermediate y axis, which coincides with the two-fold crystallographic b axis. This finding fully agrees with the recent optical absorption measurements [38] and with the phenomenological theory [25].

The phase diagram of the ANNNH model for magnetic field applied along the y axis is shown in the lower panel of Fig. 2. The commensurate AF1 state occupies a signif-

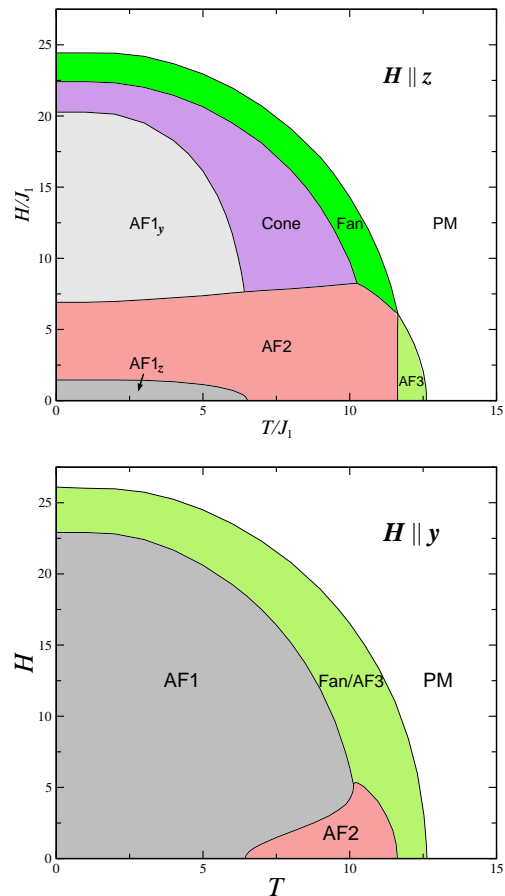


FIG. 2: The H - T phase diagrams for magnetic field along the easy z axis (upper panel) and along the intermediate y axis (lower panel). The single-ion anisotropy constants are $D = 0.3$ and $E = 0.1$.

icant part of the ordered region. In high magnetic fields the AF1 state is succeeded by the fan state. Since the spin polarization in the fan structure for $\mathbf{H} \parallel y$ is the same as in the AF3 state in zero field, the two phases are described by the same order parameter $m_{Q_{1C}}^z$ and continuously transform into each other. Overall, the theoretical diagram closely resembles the experimental diagram for $\mathbf{H} \parallel b$ [16]. The only difference between the two is a narrow strip of the magnetoelectric X phase between the AF1 and fan states present in MnWO_4 [16, 19]. This phase has a distorted cycloidal (conical) order in the ac (xz) plane and appears in our simulations for smaller values of D . The selected anisotropy parameters are, however, fixed to mimic the experimental ratio $T_{c1}/T_{c3} \approx 0.5$ in zero field. In order to fully reproduce the phase diagram of MnWO_4 for $\mathbf{H} \parallel b$ one no doubt has to consider a more realistic pattern of exchange interactions that would allow appropriate modification of anisotropy constants.

Finally, we have studied the temperature and field variations of the ordering wave vector. The published experimental data for MnWO_4 indicate close but distinct prop-

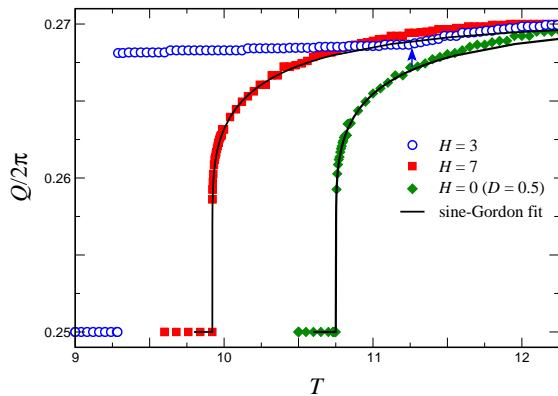


FIG. 3: Wave vector of the equilibrium magnetic structure versus temperature for $H = 3$ and 7 along the y axis ($D = 0.3$ and $E = 0.1$) and in zero field for $D = 0.5$ and $E = 0$. The solid line gives sine-Gordon fits for the direct commensurate-incommensurate transition. A small vertical arrow indicates the AF2-AF3 transition for $H = 3$.

agation vectors for the incommensurate states in zero field and above $H = 10$ T [15, 19]. Continuous variations of the ordering wave vector were also observed for TbMnO_3 [4] and $\text{RbFe}(\text{MoO}_4)_2$ [39]. From a theoretical perspective, the problem is quite challenging because discreteness of the wave vectors for a single cluster inevitably produces spurious phase transitions related to the propagation vector jumps. Instead, we have simulated a range of clusters with different linear sizes L selecting among them the magnetic structure with the lowest free energy. About 120 clusters with $10 \leq L \leq 170$ were typically investigated for each T and H . A similar approach, albeit on a lesser scale, was used previously for the ANNNI model [27].

Figure 3 shows the temperature dependence of the ordering wave vector for magnetic fields parallel to the y axis. For the $H = 3$ scan, the propagation vector exhibits a jump at the AF1–AF2 boundary accompanied by smooth weak variations inside the AF2 and AF3 phases. In zero field (not shown), Q changes even less, by only 0.5% between T_{c1} and T_{c3} . The behavior becomes notably different for scans that cross the AF1–AF3 boundary. Rapid variations of Q are clearly seen for $H = 7$ and also in zero field, once a strong easy-axis anisotropy ($D = 0.5$) suppresses the spiral phase.

The behavior of Q near the AF1–AF3 boundary can be interpreted as follows. The ordered spin components in both states are parallel to the z axis. Consequently, the free energy for the corresponding transition is expressed as a function of a complex scalar order parameter $m_{Q_C}^z(\mathbf{r})$, which is uniform in the commensurate AF1 state and acquires a position dependent phase $m_{Q_C}^z(\mathbf{r}) \sim e^{i\phi(\mathbf{r})}$ in the incommensurate AF3 state. In the constant amplitude approximation assuming slow z

variations, the free energy acquires the form

$$F = \int dz \left[\frac{K}{2} \left(\frac{d\phi}{dz} - \delta \right)^2 + \frac{V}{4} \cos 4\phi \right], \quad (3)$$

where $\delta = Q_{IC} - Q_C \approx J_1/4J_2$ and $V \propto T$ [27]. In the equilibrium state, $\phi(\mathbf{r})$ satisfies the sine-Gordon equation $\phi''_{zz} + (V/K) \sin 4\phi = 0$, which provides the basis for the analytic theory of the C – IC transition [40, 41]. Changes in the propagation vector Q are attributed to the varying distance between solitons in a periodic soliton lattice. The corresponding predictions are shown in Fig. 3 by solid lines. The excellent agreement between numerical results and the analytic theory worsens towards the Néel temperature, signifying departure from the simple $V \propto T$ law. Interestingly, there is no sign of the devil’s staircase in the temperature dependence of Q , which is known to exist for the closely related ANNNI model [26, 27]. The difference in the behavior between the two models can be related to quantum effects present in the ANNNH model and deserves further investigation.

The close resemblance of the experimental and theoretical phase diagrams suggests that the behavior of MnWO_4 in an external field is governed by competition between helicity and the bi-axial anisotropy being essentially magnetic in nature. There is no need to invoke other terms, such as a biquadratic exchange, which was suggested to play a role for $\text{Ni}_3\text{V}_2\text{O}_8$ [7]. The ferroelectricity appears as a secondary effect fully consistent with the spin current mechanism [42] with only the AF2 and the conical state showing electric polarization. The existence of the fan phase between conical and paramagnetic states confirms the observation of a non-ferroelectric magnetic phase at high fields [16]. It would be also interesting to confirm experimentally the multicritical point between fan, AF2 and AF3 phases predicted for $\mathbf{H} \parallel z$ in the present calculations and in the Landau theory [25].

Our study of the ANNNH model opens the door for a detailed theory of MnWO_4 using the multiple exchange constants deduced from high resolution inelastic neutron scattering, see, e.g., [18]. Note that the presence of long-distance exchanges in MnWO_4 improves the accuracy of the mean-field calculation for thermodynamic properties. The real-space mean-field simulations can be also applied to other multiferroic materials with complex phase diagrams. Such calculations are much simpler than the Monte Carlo simulations and, as we demonstrated, allow us to obtain temperature and field variation of the ordering wave vectors, which are not accessible in the Monte Carlo approach because the standard Metropolis algorithm does not allow for measurement of the free energy.

Acknowledgements. We thank Hiroyuki Nojiri for stimulating discussions and encouragement and appreciate helpful conversations with Björn Fåk and Efim Kats. M.E.Z. acknowledges support by the exchange program of ICC-IMR, Tohoku University.

-
- [1] S.-W. Cheong and M. Mostovoy, *Nat. Mater.* **6**, 13 (2007).
- [2] Y. Tokura, S. Seki, and N. Nagaosa, *Rep. Prog. Phys.* **77**, 076501 (2014).
- [3] R. Kajimoto, H. Yoshizawa, H. Shintani, T. Kimura, and Y. Tokura *Phys. Rev. B* **70**, 012401 (2004).
- [4] M. Kenzelmann, A. B. Harris, S. Jonas, C. Broholm, J. Schefer, S. B. Kim, C. L. Zhang, S.-W. Cheong, O. P. Vajk, and J. W. Lynn *Phys. Rev. Lett.* **95**, 087206 (2005).
- [5] G. Lawes, M. Kenzelmann, N. Rogado, K. H. Kim, G. A. Jorge, R. J. Cava, A. Aharony, O. Entin-Wohlman, A. B. Harris, T. Yildirim, Q. Z. Huang, S. Park, C. Broholm, and A. P. Ramirez, *Phys. Rev. Lett.* **93**, 247201 (2004).
- [6] G. Lawes, A. B. Harris, T. Kimura, N. Rogado, R. J. Cava, A. Aharony, O. Entin-Wohlman, T. Yildirim, M. Kenzelmann, C. Broholm, and A. P. Ramirez, *Phys. Rev. Lett.* **95**, 087205 (2005).
- [7] G. Ehlers, A. A. Podlesnyak, S. E. Hahn, R. S. Fishman, O. Zaharko, M. Frontzek, M. Kenzelmann, A. V. Pushkarev, S. V. Shiryayev, and S. Barilo, *Phys. Rev. B* **87**, 214418 (2013).
- [8] T. Kimura, J. C. Lashley, and A. P. Ramirez, *Phys. Rev. B* **73**, 220401(R) (2006).
- [9] B. X. Yang, T. R. Thurston, J. M. Tranquada, and G. Shirane, *Phys. Rev. B* **39**, 4343 (1989).
- [10] T. Kimura, Y. Seiko, H. Nakamura, T. Siegrist, and A. P. Ramirez, *Nat. Mater.* **7**, 291 (2008).
- [11] M. Kenzelmann, G. Lawes, A. B. Harris, G. Gasparovic, C. Broholm, A. P. Ramirez, G. A. Jorge, M. Jaime, S. Park, Q. Huang, A. Ya. Shapiro, and L. A. Demianets, *Phys. Rev. Lett.* **98**, 267205 (2007).
- [12] G. Lautenschläger, H. Weitzel, T. Vogt, R. Hock, A. Böhm, M. Bonnet, and H. Fuess, *Phys. Rev. B* **48**, 6087 (1993).
- [13] A. H. Arkenbout, T. T. M. Palstra, T. Siegrist, and T. Kimura, *Phys. Rev. B* **74**, 184431 (2006).
- [14] O. Heyer, N. Hollmann, I. Klassen, S. Jodlauk, L. Bohaty, P. Becker, J. A. Mydosh, T. Lorenz, and D. Khomskii, *J. Phys.: Condens. Matter* **18**, L471 (2006).
- [15] H. Nojiri, S. Yoshii, M. Yasui, K. Okada, M. Matsuda, J. -S. Jung, T. Kimura, L. Santodonato, G. E. Granroth, K. A. Ross, J. P. Carlo, and B. D. Gaulin, *Phys. Rev. Lett.* **106**, 237202 (2011).
- [16] H. Mitamura, T. Sakakibara, H. Nakamura, T. Kimura, and K. Kindo, *J. Phys. Soc. Jpn.* **81**, 054705 (2012).
- [17] H. Ehrenberg, H. Weitzel, H. Fuess, and B. Hennion, *J. Phys. Condens. Matter* **11**, 2649 (1999).
- [18] F. Ye, R. S. Fishman, J. A. Fernandez-Baca, A. A. Podlesnyak, G. Ehlers, H. A. Mook, Y. Wang, B. Lorenz, and C. W. Chu, *Phys. Rev. B* **83**, 140401(R) (2011).
- [19] I. Urcelay-Olabarria, E. Ressouche, A. A. Mukhin, V. Yu. Ivanov, A. M. Kadomtseva, Yu. F. Popov, G. P. Vorob'ev, A. M. Balbashov, J. L. Garcia-Munoz, and V. Skumryev, *Phys. Rev. B* **90**, 024408 (2014).
- [20] C. Tian, C. Lee, H. Xiang, Y. Zhang, C. Payen, S. Jobic, and M.-H. Whangbo, *Phys. Rev. B* **80**, 104426 (2009).
- [21] I. V. Solovyev, *Phys. Rev. B* **87**, 144403 (2013).
- [22] P. Toledano, B. Mettout, W. Schranz, and G. Krexner, *J. Phys.: Condens. Matter* **22**, 065901 (2010).
- [23] V. P. Sakhnenko and N. V. Ter-Oganessian, *J. Phys.: Condens. Matter* **22**, 226002 (2010).
- [24] S. Matityahu, A. Aharony, and O. Entin-Wohlman, *Phys. Rev. B* **85**, 174408 (2012).
- [25] G. Quirion and M. L. Plumer, *Phys. Rev. B* **87**, 174428 (2013).
- [26] M. E. Fisher and W. Selke, *Phys. Rev. Lett.* **44**, 1502 (1980).
- [27] P. Bak and J. von Boehm, *Phys. Rev. B* **21**, 5297 (1980).
- [28] M. Mochizuki and N. Furukawa, *Phys. Rev. B* **80**, 134416 (2009).
- [29] R. S. Fishman, G. Brown, and J. T. Haraldsen, *Phys. Rev. B* **85**, 020405(R) (2012).
- [30] R. J. Elliot, *Phys. Rev.* **124**, 346 (1961).
- [31] T. Nagamiya, in *Solid State Physics*, edited by F. Seitz, D. Turnbull, and H. Ehrenreich, (Academic, New York, 1967), Vol. 20, p. 306.
- [32] A. B. Harris, E. Rastelli, and A. Tassi *Phys. Rev. B* **44**, 2624 (1991).
- [33] A. B. Harris, *Phys. Rev. B* **76**, 054447 (2007).
- [34] D. C. Johnston, *Phys. Rev. Lett.* **109**, 077201 (2012).
- [35] P.-É. Melchy and M. E. Zhitomirsky, *Phys. Rev. B* **80**, 064411 (2009).
- [36] R. P. Chaudhury, B. Lorenz, Y. Q. Wang, Y. Y. Sun, and C. W. Chu *Phys. Rev. B* **77**, 104406 (2008).
- [37] F. Ye, Y. Ren, J. A. Fernandez-Baca, H. A. Mook, J. W. Lynn, R. P. Chaudhury, Y.-Q. Wang, B. Lorenz, and C. W. Chu, *Phys. Rev. B* **78**, 193101 (2008).
- [38] S. Toyoda, N. Abe, T. Arima, S. Kimura, *Phys. Rev. B* **91**, 054417 (2015).
- [39] H. Mitamura, R. Watanuki, K. Kaneko, N. Onozaki, Y. Amou, S. Kittaka, R. Kobayashi, Y. Shimura, I. Yamamoto, K. Suzuki, S. Chi, and T. Sakakibara, *Phys. Rev. Lett.* **113**, 147202 (2014).
- [40] I. E. Dzyaloshinskii, *Sov. Phys. JETP* **20**, 665 (1965).
- [41] P. M. Chaikin and T. C. Lubensky, *Principles of Condensed Matter Physics* (Cambridge University Press, Cambridge, UK, 1995).
- [42] H. Katsura, A.V. Balatsky and N. Nagaosa, *Phys. Rev. Lett.* **98**, 027203 (2007).